Bioinspiration &
Biomimetics

PAPER • **OPEN ACCESS**

BlueGuppy: tunable kinematics enables maneuverability in a minimalist fish-like robot

To cite this article: Hungtang Ko *et al* 2025 *Bioinspir. Biomim.* **20** 056006

Bioinspiration & Biomimetics

PAPER

BlueGuppy: tunable kinematics enables maneuverability in a minimalist fish-like robot

Hungtang Ko[1,*], Valeria Saro-Cortes[1], Brian Mmari[2], Di Ni[1], Aimy Wissa[1] and Radhika Nagpal[1,3]

[1] Department of Mechanical and Aerospace Engineering, Princeton University, Princeton, NJ 08540, United States of America
[2] Department of Electrical and Computer Engineering, Princeton University, Princeton, NJ 08540, United States of America
[3] Department of Computer Science, Princeton University, Princeton, NJ 08540, United States of America
[*] Author to whom any correspondence should be addressed.

E-mail: hk1581@princeton.edu

Keywords: bioinspired robotics, fluid mechanics, maneuverable, miniature

Supplementary material for this article is available online

OPEN ACCESS

RECEIVED
7 May 2025

REVISED
26 June 2025

ACCEPTED FOR PUBLICATION
22 July 2025

PUBLISHED
21 August 2025

Abstract

Aquatic ecosystems vital to biodiversity and climate change—such as coral reefs, kelp forests, and mangrove forests—are often cluttered with natural obstacles. To navigate these complex habitats, fish have evolved relatively small body sizes and outstanding maneuverability. In contrast, most unmanned underwater vehicles currently deployed for ocean monitoring are bulky and slow, limiting their ability to access these environments. Developing small and agile underwater robots that mimic native fish species provides a unique opportunity for automated sampling of dynamic aquatic ecosystems. In this paper, we present BlueGuppy, a miniature, low-cost, and untethered fish-like robot ($9.5 \times 2.4 \times 3.0$ cm, 33.1 g) capable of maneuvering with a single actuator. It achieves swimming speeds of up to 2.8 body lengths per second and can execute tight turns with small circles 1.4 body lengths in radius. BlueGuppy can generate a net thrust even in the presence of an incoming flow, but the flow field around BlueGuppy only mirrors that of biological organisms when it is free-swimming, underscoring the importance of untethered robots for biomimetic research. We explored the maneuverability of BlueGuppy by tuning its kinematics. By varying its flapping frequencies and temporal bias, BlueGuppy can access a wide range of speeds and turning curvatures. The combination of speed, maneuverability, and simplicity establishes BlueGuppy as a unique platform in the literature with tremendous potential for both uncovering the biomechanics of schooling fish and advancing the state-of-the-art in autonomous ocean sampling.

1. Introduction

Fish demonstrate exceptional maneuverability as they traverse complex aquatic environments such as coral reefs, kelp forests, and mangrove forests. These ecosystems are characterized by high structural complexity and biodiversity, with dense aquatic vegetation providing essential shelters for juvenile and small-bodied fish species. These aquatic plants also contribute to carbon sequestration and play a role in global climate regulation [1–3]. However, many of these ecosystems are increasingly threatened by anthropogenic pressures, and current monitoring capabilities remain limited. Existing unmanned underwater vehicles are typically bulky, limiting their ability to effectively navigate and collect data within these highly cluttered environments. In contrast, fish native to these habitats navigate natural obstacles gracefully, taking advantage of their small body size and agility.

Fish-like robots provide a promising solution to navigating these complex aquatic environments [4–18]. Compared to traditional propeller-based unmanned underwater vehicles (UUV), flapping-based robots are less prone to producing cavitation bubbles which not only produce underwater noise but can also cause structural damage over time. Fish-like robots also hold the potential of biomimicry, harnessing the efficient individual or group locomotion strategies that fish have developed over hundreds of millions of years of evolution. They may be used to test biomechanical hypotheses of fish movement, to research the functions of different fishes' morphology

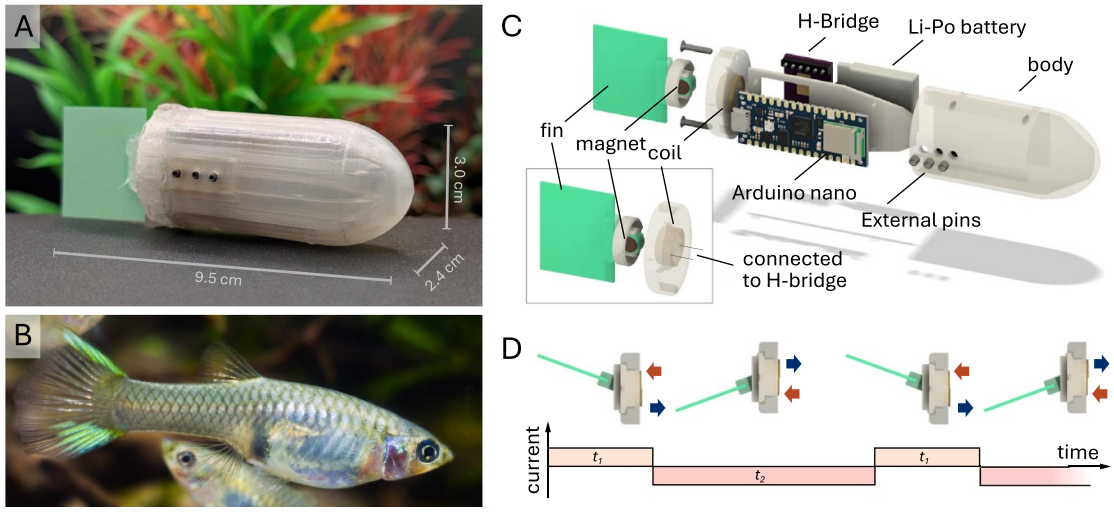

Figure 1. Design of BlueGuppy, a minimalist fish-like maneuverable robot. (A) Photos of BlueGuppy and (B) a guppy (adobe stock). (C) Components and assembly of BlueGuppy. Inset shows a zoomed-in image of the actuator. (D) BlueGuppy's only actuator flaps with a temporal bias when duration of positive and negative current $t_1 \neq t_2$.

and kinematics, and to explore the hydrodynamic interaction among schooling fish.

Fish-inspired robotics research has primarily focused on straight-line swimming performance [10–12, 18]. However, maneuverability in underwater robots presents a different challenge. To be agile, a robot needs to have a small body to minimize inertia and be able to turn with different curvatures at speed. Intuitively, turning can be achieved by having multiple actuators. BlueBot, one of the earliest maneuverable fish-like robots, uses two actuators in addition to its main propulsive actuator to control its turning. It can successfully trace a square-shaped trajectory [5] and perform complex collective maneuvers such as the evasive fountain [7] and circular milling [6]. Other fish robots also use similar strategies to turn in their environments [13, 19–26]. However, the use of multiple actuators complicates the design, and an increase in size is often necessary, defeating the goal of improving agility.

In contrast, while fish often engage multiple fins to hover in place and perform gentle maneuvers [27], they rely mainly on their caudal fins and body deformation in explosive turns [28–31]. Whether flapping robots can achieve maneuverability using a single actuator remains a compelling challenge. Conventional actuators, such as motors and propellers, typically exert force unidirectionally, thus controlling one degree of freedom [10, 11]. Conversely, biomimetic flapping-based actuators generate forces through nonlinear interactions with the surrounding fluid, providing a unique opportunity for versatile control. Notably, studies on flapping hydrofoils have demonstrated that spatial and temporal asymmetries can be exploited to produce lateral forces and pitching moments [32, 33], and biological organisms indeed utilize temporal asymmetry for turning [30, 31]. Applying these control strategies to a minimalistic robotic fish could enable agile maneuvering with only one actuator, representing a significant advancement in bio-inspired robotics.

The primary contribution of this work is the development of BlueGuppy, a novel, fish-like robot that advances the field in several key ways. First, BlueGuppy is among the first fish-inspired platforms to combine small size, untethered operation, and high maneuverability, enabling new experimental possibilities in complex aquatic environments. Second, it is capable of generating biologically relevant wakes, providing researchers with a valuable tool for studying hydrodynamic interaction between fish. Third, BlueGuppy leverages tunable kinematics, allowing it to access a wide range of turning curvatures and speeds, which further broadens its applicability in both biological research and robotics. The design and unique characteristics of BlueGuppy, which collectively represent a significant step forward in bio-inspired robotics, are detailed in the following sections.

2. Methods

2.1. BlueGuppy design

This BlueGuppy project explores the simplest design that enables high swimming performance and maneuverability. BlueGuppy is 9.5 cm long (including the fin), 2.4 cm wide, and 3.0 cm tall (figure 1(A)). It weighs 33.1 g. Its center of mass is lower than the center of pressure, so that the robot is passively stable in both roll and pitch. It is also slightly buoyant. When not actuated, BlueGuppy floats at the air–water interface with less than 5% of its body above water. BlueGuppy is inspired by the miniature size

and exceptional maneuverability of guppies (*Poecilia reticulata*), also known as rainbow fish (figure 1(B)).

The main components of the BlueGuppy are shown in figure 1(C). Arduino Nano is used as the micro-processing unit of the circuit, which can be programmed over-the-air so that the fish robot can be permanently sealed and does not need to be reopened. The chip can also handle commands through its wireless modules, such as WiFi and bluetooth. It is always connected to the battery, but is in the deep sleep mode to minimize the current drawn when idle. The board wakes up when two of the external pins (figure 1(C)) are shorted, and starts to actuate when the pins are shorted again. The third external pin is used to charge the battery.

BlueGuppy uses a custom magnet-in-coil actuator at its tail (figures 1(C) and (D)) [5, 6, 34, 35]. To actuate BlueGuppy, the microcontroller sends an alternating current to the coil through the H-bridge (figure 1(D)). The alternating current induces an alternating magnetic field, creating a torque that aligns the permanent magnet periodically. This results in flapping movement of the tail fin, which is made of a 2.4 cm by 3.0 cm plastic shim stock with a 0.08 mm thickness. In this study, we used square waves with equal magnitudes to actuate BlueGuppy (figure 1(D)). The durations when the current was positive, t_1, and negative, t_2, are two free parameters that we studied. These parameters can be changed based on the wireless commands sent to the Arduino.

2.2. Force measurement

We characterized BlueGuppy's performance in a water channel with a cross-section 45 cm wide and 30 cm deep (figure 2(A)), similar to the setup in [36]. A BlueGuppy, flapping symmetrically at 10 Hz, was connected to an attachment rod close to its geometric center, which was mounted to a six-axis force transducer (AIT nano 17 Titanium SI-8-0.05). The force signals were transmitted through a data acquisition device (DAQ) (NI USB-6212) to a computer. In addition, we measured the force generated by the BlueGuppy when the it was idle and when no BlueGuppy was attached at all. The latter was used as a baseline to account for the drift in the force transducer. The drag in figure 2(C) represented the streamwise force (x-axis) experienced by an idle robot body, and the thrust was calculated as the difference between the streamwise force experienced by an actuated and an idle robot. Thus, the thrust represented the hydrodynamic consequence of the propulsor flapping at 10 Hz. For each condition, we used a custom MATLAB script to collect the data for ten seconds, or 100 cycles. A postprocessing script then subtracted all the force data by the drift and performed cycle-averaging across every two cycles (0.2 s)

We placed BlueGuppy in five different incoming flow speeds from 12.8 to 28.8 cm s^{-1}. This speed range included the free-swimming speed of BlueGuppy at 26.6 cm s^{-1}. As a result, as we show in the Results section, rigidly-attached BlueGuppy transitioned from generating thrust to generating drag. This transition occurred at approximately 20.8 cm s^{-1}, when the tethered BlueGuppy experienced almost no net force in a flapping cycle. This speed range also falls into the operating range of our water channel, ensuring that the flow experienced by BlueGuppy was laminar.

Due to the symmetry of the setup, the force measured was approximately planar, with a negligible force in the vertical axis along the rod (z-axis). The moments in the horizontal direction closely mirrored the forces, i.e. $M_x = F_y \cdot l$ and $M_y = F_x \cdot l$, where l is the length of the attachment rod and the moment arm. With a relatively long moment arm $l \approx 19$ cm, the torque channels provided a much better signal-to-noise ratio and were used to calculate the F_x and F_y below.

With this method, our data acquisition had a range of 0–2.6 N and a resolution of 0.0004 N. The data presented below was well within this range and the means separated beyond the limit of resolution. Thus, variations in our measurements (e.g. figure 2(C)) were caused by factors such as the imperfection of flow and robot assembly. To verify that the means of our force measurements differ significantly despite the standard deviation, we conducted 1-way ANOVA tests and Tukey's HSD tests.

2.3. Flow field characterization

The wake of BlueGuppy was extracted using planar Particle Imagery Velocimetry (PIV). The setup included a dual-headed pulsed laser (Litron nano LPV 50–50) and a high-speed camera (Photron Nova FastCam R5). The laser was equipped with a converging lens, a diverging lens, and a Powell lens for focusing and flattening the laser beam into a sheet. The flow was seeded with 10 μm hollow glass spheres for visualization. We used DaVis 10 to record and process the flow field. For all our experiments, we measured the flow field at a 50 fps frequency by taking paired images with a resolution of 4096 $\times$ 2304 pixels. The flow field was recorded for five seconds, or 50 cycles, and averaged every cycle to reduce noise. We measured jet angles by manually annotating the locations of the first few vortices in each of the two jets behind BlueGuppy. For each condition, the deflection angles of the two jets are similar, and we report the average value below.

2.4. Maneuverability tests

We conducted a series of maneuverability tests in a stationary-water pool 218 cm (23 body lengths) wide and 124 cm (13 body lengths) long (Intex). The water was 30 cm deep. A GoPro was mounted above the pool to capture its top view at 120 frames per second,

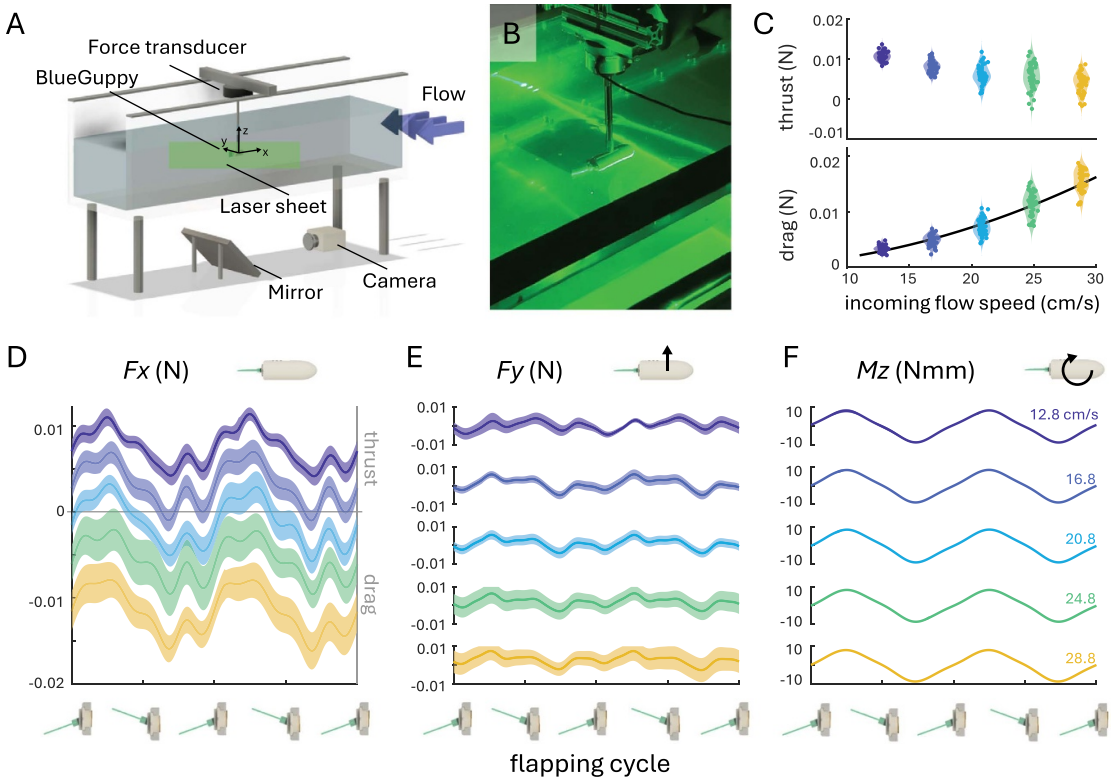

Figure 2. Rigidly-held BlueGuppy generates thrust in flow. (A) Schematic and (B) photo of the experimental setup. (C) Thrust from BlueGuppy's tail and drag from the main body at different flow speeds. The black line represents $\frac{1}{2}C_D A_\rho U^2$, where A is the cross-section area of BlueGuppy, ρ the water density, and U the incoming flow speed. Here, $C_D = 0.5$. (D) Net stream-wise force F_x, (E) lateral force F_y, and (F) torque M_z over two cycles. Colors indicate different flow speeds, and the shade represents the standard deviation across 25 additional cycles.

and the floor of the pool was covered with black acrylic sheets to improve contrast. For each combination of actuation timings t_1 and t_2, we sent a wireless command to BlueGuppy to change its kinematics and placed it in the water at least three times in the pool. Due to the large surface area of the pool, BlueGuppy swam uninterrupted from five seconds to 60 s.

2.5. Video processing

We developed a custom contrast-based video-processing program in MATLAB to track BlueGuppy's states, i.e. body angle, centroid coordinates, and their derivatives. First, the program applied a constant threshold to binarize each frame and removed areas much smaller than the robot fish. Only one blob remained at this stage, representing the group of pixels that BlueGuppy occupied. Then, we calculated the centroid and orientation of this blob and repeated this process for every frame. Once the full time series of the robot's state was extracted, its translational and angular velocities were calculated by taking time derivatives. We did not directly calculate the turning curvature by using the second derivatives, which were noisy. Instead, taking advantage of the circular geometry, we calculated local curvature as the ratio between angular and translational velocities. The turning curvature and speed were approximately constant throughout the trajectory, and we used the median values as the representative metrics for each kinematic condition.

3. Results

3.1. Hydrodynamics of tethered and free-swimming BlueGuppies

BlueGuppy produces thrust regardless of the flow conditions (figure 2(C)). The thrust, calculated as the difference between the streamwise force experienced by an actuated BlueGuppy and an idle BlueGuppy, is always positive, suggesting that the flapping actuator can provide propulsion in all swimming speeds. The thrust is higher at lower speeds (ANOVA: $p < 0.001$), so a free-swimming robot would experience the most acceleration when started from rest. The thrust decreases as the incoming flow speed increases, or as a free-swimming BlueGuppy swims at higher speeds. Due to its streamlined body shape, BlueGuppy has only approximately 3.3 mN drag at 12.8 cm s^{-1}. The drag increases significantly with the flow speed (ANOVA: $p < 0.001$). It scaled with the speed squared, indicating that the pressure drag is the main source. This is expected since the Reynolds number of BlueGuppy exceeds 10^4 and inertial effects dominate over viscous effects. The

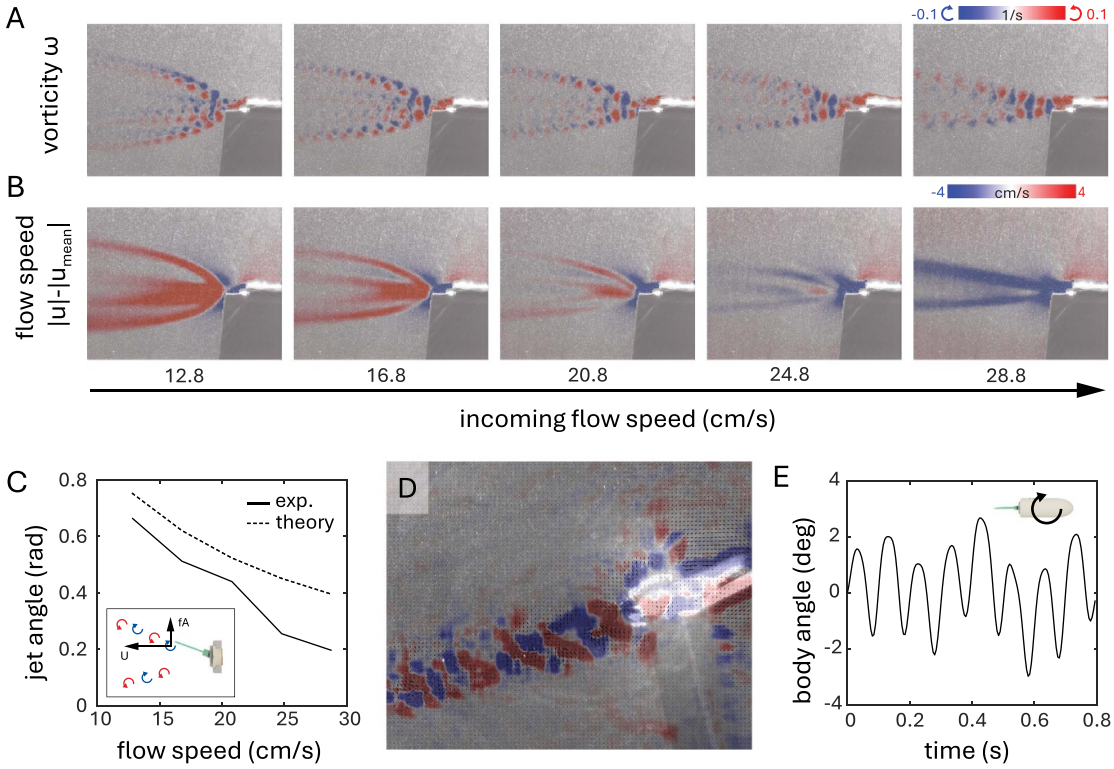

Figure 3. Rigidly-held BlueGuppy produces bifurcating wakes. (A) The vorticity field and (B) the flow field of BlueGuppy across five different flow speeds. (C) Jet angle as a function of flow speed in experiments and in theory. (D) Free-swimming BlueGuppy produces a single vortex street similar to fish. (E) Body angle of the free-swimming BlueGuppy.

drag coefficient C_D of an idle BlueGuppy body is approximately 0.5.

Figures 2(D)–(F) demonstrates the streamwise force (figure 2(D)), lateral force (figure 2(E)), and the turning torque (figure 2(F)) of a rigidly-held BlueGuppy over two periods when it flaps at 10 Hz. All forces fluctuate periodically, but except for the torque M_z, the fluctuations of F_x and F_y are slightly irregular, possibly due to the imperfections of the setup. Combining the drag from the body and the propulsion from the tail, the net force experienced by the BlueGuppy in the x direction decreased from a positive to a negative value. This indicates that as the speed of the incoming flow increases from 12.8 cm s^{-1} to 28.8 cm s^{-1}, the rigidly-held BlueGuppy transitions from producing thrust to producing drag. The force is approximately balanced when the incoming flow is at 20.8 cm s^{-1}. The lateral force and the torque are insensitive to the flow speed.

The vorticity and the flow generated by a rigidly-held BlueGuppy are shown in figures 3(A) and (B) and the supplemental video. The periodic flapping motion of BlueGuppy creates vortices in alternating directions behind it, leaving a bifurcating wake. When the incoming flow speed is low (12.8 cm s^{-1}), BlueGuppy generates a net thrust and increases the speed of the fluid around it (figure 3(B)). When the incoming flow speed is high (28.8 cm s^{-1}), BlueGuppy slows down the flow and leaves two angled trails. As expected from momentum balance, when the force is balanced at an intermediate flow speed (20.8 cm s^{-1}), BlueGuppy is almost invisible to the flow, leaving virtually no perturbations at all at just one body length downstream (figure 3(B)). The speeds of the wake in figure 3(B) match well with the arrangement of vortices in figure 3(A). When BlueGuppy accelerates the flow at 12.8 cm s^{-1}, most clockwise vortices (blue) are above the counterclockwise vortices (red). This relationship is reversed when BlueGuppy decelerates the flow at 28.8 cm s^{-1}.

Notably, the rigidly-held BlueGuppy always produces bifurcating wakes regardless of the flow condition. As the incoming flow speed increases, the angle of the jet decreases (figure 3(A)). Here, we provide a simple rationale for this deflection. When the vortices are shed, they are advected according to the local velocity field. The velocity along the stream (x-axis) is approximately U, the speed of the incoming flow. The lateral velocity across the stream (y-axis) is roughly the speed of the flapping tail moving from side to side, scaling with $f \cdot A$, where f is the flapping frequency and A the amplitude. Thus, we expect the jet deflection angle $\theta_{\text{jet}} = \arctan(\frac{fA}{U}) = \arctan(\text{St})$, where St is the Strouhal number, a dimensionless parameter often used to characterize the flow generated by a periodic

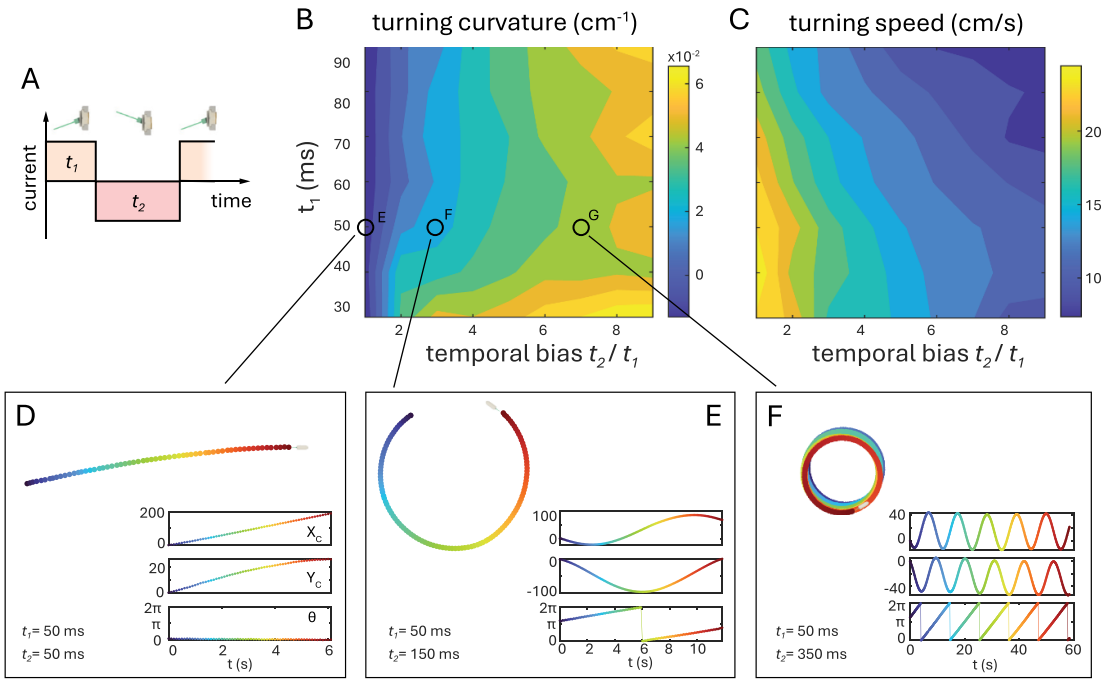

Figure 4. Asymmetric flapping leads to turning in BlueGuppy. (A) Schematic of the temporal asymmetry introduced in BlueGuppy. Contours of (B) turning curvature and (C) speed as BlueGuppy's actuation timing t_1 and bias t_2/t_1 vary. Positive curvatures suggest left-turning. Representative trajectories of BlueGuppy with (D) no bias, (E) low bias, and (F) high bias. Insets show time series of its centroid displacements and orientations.

flapping motion. Figure 3(C) shows that this simple theory qualitatively explains the variation of the jet angles in our experiments.

The bifurcating wake pattern observed in the rigid-held BlueGuppy is distinct from the reverse Karman vortex street that fish produce [4], a single streak of alternating vortices. BlueGuppy generates this wake only when it swims freely (figure 3(D)). The stark difference between the wake generated by a free-swimming BlueGuppy and a rigidly-held BlueGuppy at similar relative flow speeds highlights the effect of constraining the robot fish. The rigid attachment transmits periodic streamwise (figure 2(D)) and lateral (figure 2(E)) forces as well as a significant yawing torque (figure 2(F)) that free-swimming BlueGuppy does not experience. Instead, free-swimming BlueGuppy adapts to the hydrodynamic forces it generates: it fluctuates its body angle periodically as it swims (figure 3(E)), mirroring the yawing motion of fish [37].

3.2. Tunable kinematics enables maneuverability in BlueGuppy

The locomotion of a free-swimming BlueGuppy is fully decided by its kinematics, which can be tuned in our system. We explore BlueGuppy's behavior as we systematically vary the timing of its control, introducing a temporal bias t_2/t_1 to break the left–right symmetry (figure 4(A)). Figures 4(B) and (C) and the supplemental video demonstrate that BlueGuppy can turn at a wide range of curvatures using its only actuator. When there is no temporal bias $t_2/t_1 = 1$, BlueGuppy swims along a straight line (figure 4(D)). With a small temporal bias $t_2/t_1 = 3$, BlueGuppy turns with a small curvature 0.023 cm^{-1}, or with a turning radius 1/0.023 = 43.5 cm, 4.6 its body lengths (figure 4(E)). Its turning radius decreases as the temporal bias increases. At $t_2/t_1 = 7$, BlueGuppy turns at a much tighter circle with a radius of 21.9 cm, 2.3 its body lengths (figure 4(F)). This turning is remarkably robust. BlueGuppy completes five full revolutions within a minute, with circular trajectories overlapping with themselves (figure 4(F)). BlueGuppy executes the tightest turn at the highest temporal bias. At minimum, it can turn in circles as small as 13.6 cm in radius, or 1.4 body lengths.

Varying the kinematics also affects the turning speeds (figure 4(C)). At its characteristic swimming frequency of 10 Hz ($t_1 = t_2 = 50$ ms), BlueGuppy swims at 24.4 cm s^{-1} or 2.6 body lengths per second. The swimming speed mainly depends on its effective flapping frequency $\frac{1}{t_1+t_2}$ and varies smoothly even when it is turning (figure 5(A)). The swimming speed is the fastest when the fish is flapping symmetrically at 12.5 Hz ($t_1 = t_2 = 40$ ms), at 26.2 cm s^{-1} or 2.8 body lengths per second. BlueGuppy's speed U increases approximately with the frequency f to the one-half power. This is surprising because biological swimmers often have a constant Strouhal number $St = fA/U$ [4, 38] and amplitude A [39]. Consequently,

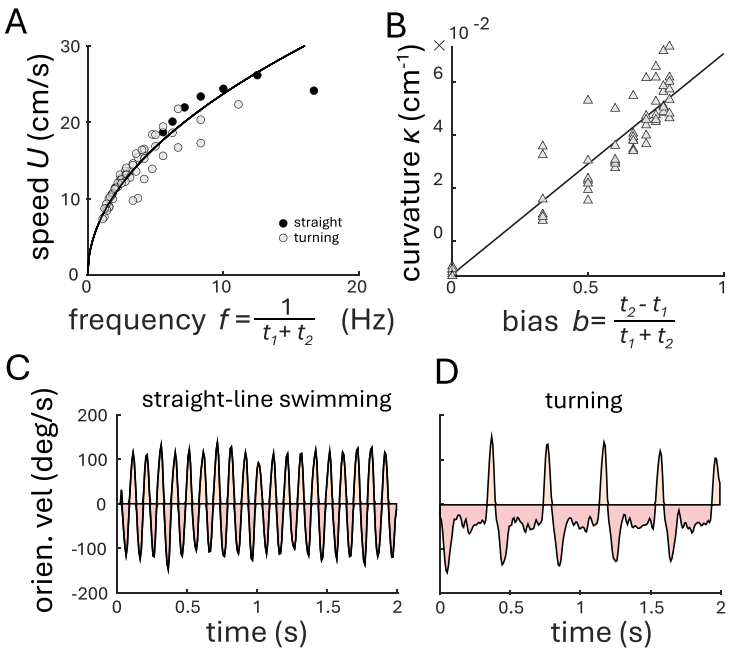

Figure 5. (A) Speed of BlueGuppy while swimming straight (filled dots) and turning (open dots). Black line shows a trend line $U = 0.75f^{0.5}$ (B) Curvature of BlueGuppy's trajectory as a function of the bias. The straight line $\kappa = -0.013 + 0.083b$ shows the best fit. (C)–(D) Orientational velocities of BlueGuppy during (C) straight-line swimming and (D) turning in representative trajectories. The experimental condition in (C) is the same as figure 4(D) ($t_1 = t_2 = 50$ ms), and (D) the same as figure 4(F) ($t_1 = 50$ ms, $t_2 = 350$ ms).

their swimming speed U increases linearly with the tail-beat frequency f [39]. BlueGuppy's swimming speed increases more slowly with frequency because while fish actively control for their tail amplitude, BlueGuppy's amplitude A decreases with frequency f due to the tail's flexibility.

Figures 5(B)–(D) reveals the mechanism of BlueGuppy's turning. Symmetrically actuated BlueGuppy generates a periodically oscillating orientational velocity (figure 5(C)). Flapping towards each side creates the same peak orientational velocity around 100 deg s^{-1}. The change in BlueGuppy's orientation, i.e. the area under the curve in figure 5(C), is zero for each cycle. With a temporal bias, there is a net change in direction for each cycle, leading to turning (figure 5(D)). Because the direction change in the electrical current, and thus the magnetic field of the coil, is almost instantaneous, the peak orientational velocity generated is insensitive to the temporal bias, at approximately 130 deg s^{-1}(figure 5(C) and (D)). The widths of the main peaks are also similar, around t_1, or 50 ms. When the tail is held on one side during biased turning, BlueGuppy coasts with a small orientational velocity of around 50 deg s^{-1} after the initial burst. This phase lasts for $t_2 - t_1$ and is the main contributor to the persistent turning of BlueGuppy. We redefine the bias b as the ratio between this period and the period of oscillation, $b = \frac{t_2 - t_1}{t_1 + t_2}$ and show that it is directly correlated with the curvature of BlueGuppy's trajectory (figure 5(B)). This suggests that the turning mechanism of BlueGuppy is drag-based, and the tail acts as a rudder on a boat. Even just for a fraction of a second in each cycle, this can result in significant turning of the robot.

4. Discussion

In this paper, we present BlueGuppy, a minimalist robot that generates fish-like movement and is highly maneuverable. We explored the hydrodynamics of a rigidly-held BlueGuppy, showing that it can generate thrust and create bifurcating wakes that are distinct from free-swimming BlueGuppy. Furthermore, we demonstrate its ability to maneuver, showing how temporal bias can be introduced in this simple actuator to facilitate drag-based turning.

To our knowledge, BlueGuppy is one of the first fish-like robots that is miniature, untethered, and highly maneuverable. While aquatic bio-inspired robots have attracted considerable attention, few can match the performance of BlueGuppy. Most existing robots have limited speeds, typically with maximal straight-line velocities of less than one body length per second [11], much slower than BlueGuppy. Recent work has pushed these speed limits [10, 12–14]. One of the fastest fish robots, Tunabot flex, achieved an impressive speed of 4.6 body lengths per second [11]. However, like most fish-like robots that focus on swimming performance, Tunabot flex is tethered—its power is delivered via external wires, and its body lacks an onboard battery and microcontroller. Furthermore, it cannot turn using its tail,

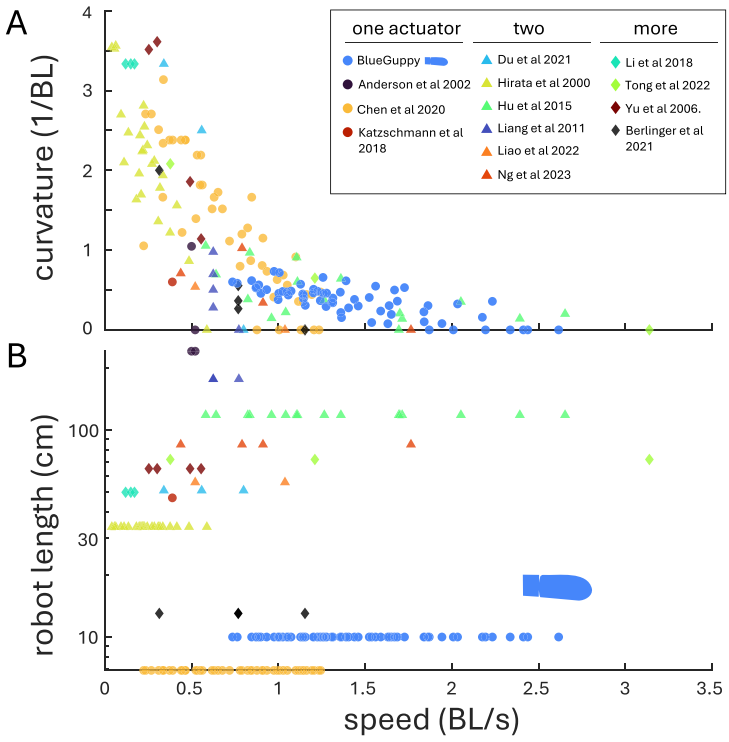

Figure 6. Turning curvatures and speeds achieved by underwater robots in current literature.

limiting its maneuverability and applications in open water environments.

BlueGuppy's maneuverability puts it in a unique position in the fish robot literature, as shown in figure 6 [6, 19–26, 40–43], where we have excluded robots that are unable to turn. Notably, there is a trade-off between achieving a high turning curvature and maintaining a high speed (figure 6(A)). To facilitate extremely tight turns, many fish-like robots turn while having virtually no translational speed [6, 15–18]. However, agile maneuvers in the field often require turning at high speeds, and achieving a balance between high curvature and speed is crucial for quickly completing a planned trajectory. Most turning fish robots in the literature also have more than one actuator and are much larger than BlueGuppy (figure 6(B)). Due to the complexity of some turning mechanisms and the number of actuators required, with the exception of Chen *et al* [41], Berlinger *et al* [6], and BlueGuppy, all turning robots are significantly longer than ten centimeters, some reaching a meter in length, making it challenging to maneuver in cluttered natural environments such as coral reefs and kelp forests.

A key factor in BlueGuppy's performance is its magnet-in-coil actuator (figure 1(D)). Compared to other actuators commonly used in fish robots, such as the DC motors used in TunaBots [10, 11] and the hydraulic pump systems used in SoFi [42], our actuator is compact, easy to waterproof, and supports high actuation frequencies. While BlueGuppy's predecessor, Bluebot, showcased the scalability of the actuator, with multiple actuators mounted on a compact body, BlueGuppy further demonstrates its versatility. By incorporating a temporal bias and tunable kinematics, a single actuator can provide high maneuverability. How the shape and stiffness of the attached fin influence the actuator's force generation capabilities remains an exciting research question with significant biological relevance.

Our results also highlight the value of free-swimming robots in researching the hydrodynamic interactions among multiple swimmers, such as fish in a school. The fluid mechanics of fish schools has long been a topic of interest, and rigidly-held hydrofoils are often used in experiments to recreate the flow of swimming fish [4]. However, while free-swimming individuals are not subject to any external forces, an external pitching torque is required to generate the flapping motion of hydrofoils. The added torque, as well as the constraint in lateral movement, can create artifacts in the flow field that are distinct from the free-swimming individuals, as we showed in figure 2. To study the hydrodynamic interactions among schooling fish, it may be essential to use free-swimming robots such as BlueGuppy.

More generally, free-swimming and maneuverable robots like BlueGuppy present unique opportunities for studying underwater collective behavior. Tethered robots cannot be deployed in large numbers due to cable entanglement, and ground robots do not experience the complex fluid force aquatic collectives

do. The maneuverability of fish-like robots also allows research into 3D formation control [8, 9, 44] and collective maneuvers such as milling (turning in circles together) [6] and predator avoidance [7]. The hydrodynamic interactions in these natural collective behaviors of fish and the role of their various sensing modalities remain an active area of research in both biology and engineering [4].

Future research is required to explore how the maneuverability of fish-like robots translates to natural environments. Marine ecosystems crucial to the climate and biodiversity, such as coral reefs, mangrove forests, and kelp forests, are often cluttered with natural obstacles. Miniature and maneuverable robots may help monitor these environments, but overcoming unpredictable currents and waves may be challenging. Researching how individual fish robots may sense the variable flow environment and adapt to it, and how groups of fish robots may shelter each other from the external fluid disturbances like schooling fish [39], are exciting future directions to pursue.

Data availability statement

All data that support the findings of this study are included within the article (and any supplementary files).

Acknowledgments

We acknowledge support from ONR MURI Grant N00014-22-1-2616 (co-PI R Nagpal), James S McDonnell Foundation's Postdoctoral Fellowship for Understanding Dynamic & Multi-scale Systems (PI H Ko), and the Princeton SEAS Innovation Research Grant.

Citation diversity statement

This statement is inspired by a recent initiative (Zurn *et al* https://doi.org/10.1016/j.tics.2020.06.009) and recent studies that revealed the under-representation and under-citation of women, non-white, and other marginalized scholars (Teich *et al* https://doi.org/10.1038/514s41567-022-01770-1). Here, we provide a breakdown of our references using the tool https://github.com/dalejn/cleanBib, excluding self citations. Our references contain 5.4% woman(first author)/woman(last author), 13.5% man/woman, 18.9% woman/man, and 62.2% man/man. By race, our references contain 37.8% POC(first)/POC(last), 5.4% White/POC, 18.9% POC/White, and 37.8% White/White. Most People of Color (POC) cited are Asian. This method is limited in that names are imperfect predictors of race and gender; Marginalized groups such as non-binary, transgender, Black, Indigenous, and mixed-race are difficult to identify. We look forward to future work that better supports equitable practices in science.

ORCID iDs

Hungtang Ko 0000-0001-6250-6144
Valeria Saro-Cortes 0000-0003-3009-1049
Di Ni 0009-0009-4851-7862
Aimy Wissa 0000-0002-8468-511X
Radhika Nagpal 0000-0001-9756-0167

References

[1] Mcleod E, Chmura G L, Bouillon S, Salm R, Björk M, Duarte C M, Lovelock C E, Schlesinger W H and Silliman B R 2011 A blueprint for blue carbon: toward an improved understanding of the role of vegetated coastal habitats in sequestering CO2 *Front. Ecol. Environ.* **9** 552–60
[2] Krause-Jensen D and Duarte C M 2016 Substantial role of macroalgae in marine carbon sequestration *Nat. Geosci.* **9** 737–42
[3] Rosentreter J A *et al* 2023 Coastal vegetation and estuaries are collectively a greenhouse gas sink *Nat. Clim. Change* **13** 579–87
[4] Ko H, Lauder G and Nagpal R 2023 The role of hydrodynamics in collective motions of fish schools and bioinspired underwater robots *J. R. Soc. Interface* **20** 20230357
[5] Berlinger F, Dusek J, Gauci M and Nagpal R 2018 Robust maneuverability of a miniature, low-cost underwater robot using multiple fin actuation *IEEE Robot. Autom. Lett.* **3** 140–7
[6] Berlinger F, Gauci M and Nagpal R 2021 Implicit coordination for 3D underwater collective behaviors in a fish-inspired robot swarm *Sci. Robot.* **6** eabd8668
[7] Berlinger F, Wulkop P and Nagpal R 2021 Self-organized evasive fountain maneuvers with a bioinspired underwater robot collective *2021 IEEE Int. Conf. on Robotics and Automation (ICRA)* pp 9204–11
[8] Salazar J, Cai L, Cook B and Rus D 2022 Multi-robot visual control of autonomous soft robotic fish *2022 IEEE/OES Autonomous Underwater Vehicles Symp. (AUV)* pp 1–6
[9] Zhang Z, Yang T, Zhang T, Zhou F, Cen N, Li T and Xie G 2021 Global vision-based formation control of soft robotic fish swarm *Soft Robot.* **8** 310–8
[10] Zhu J, White C, Wainwright D K, Di Santo V, Lauder G V and Bart-Smith H 2019 Tuna robotics: a high-frequency experimental platform exploring the performance space of swimming fishes *Sci. Robot.* **4** eaax4615
[11] White C H, Lauder G V and Bart-Smith H 2021 Tunabot flex: a tuna-inspired robot with body flexibility improves high-performance swimming *Bioinsp. Biomim.* **16** 026019
[12] Zhong Q, Zhu J, Fish F E, Kerr S J, Downs A M, Bart-Smith H and Quinn D B 2021 Tunable stiffness enables fast and efficient swimming in fish-like robots *Sci. Robot.* **6** eabe4088
[13] Clapham R J and Hu H 2014 iSplash-II: realizing fast carangiform swimming to outperform a real fish *2014 IEEE/RSJ Int. Conf. on Intelligent Robots and Systems* (*Chicago, IL, USA*IEEE) pp 1080–6
[14] van den Berg S C, Scharff R B N, Rusák Z and Wu J 2022 OpenFish: biomimetic design of a soft robotic fish for high speed locomotion *HardwareX* **12** e00320
[15] Deng H, Li D, Panta K, Wertz A, Priya S and Cheng B 2024 Effects of caudal fin stiffness on optimized forward swimming and turning maneuver in a robotic swimmer *Bioinsp. Biomim.* **19** 036003
[16] Zhong Y, Li Z and Du R 2017 A novel robot fish with wire-driven active body and compliant tail *IEEE/ASME Trans. Mechatronics* **22** 1633–43
[17] Marchese A D, Onal C D and Rus D 2014 Autonomous soft robotic fish capable of escape maneuvers using fluidic elastomer actuators *Soft Robot.* **1** 75–87

[18] Iguchi K, Shimooka T, Uchikai S, Konno Y, Tanaka H, Ikemoto Y and Shintake J 2024 Agile robotic fish based on direct drive of continuum body *npj Robot.* **2** 1–9
[19] Du S, Wu Z, Wang J, Qi S and Yu J 2021 Design and control of a two-motor-actuated tuna-inspired robot system *IEEE Trans. Syst. Man Cybern.: Syst.* **51** 4670–80
[20] Hirata K, Takimoto T and Tamura K 2000 Study on turning performance of a fish robot *First International Symposium on Aqua Bio-Mechanisms* (Honolulu.) pp 287–92
[21] Liang J, Wang T and Wen L 2011 Development of a two-joint robotic fish for real-world exploration *J. Field Robot.* **28** 70–79
[22] Liao X, Zhou C, Zou Q, Wang J and Lu B 2022 Dynamic modeling and performance analysis for a wire-driven elastic robotic fish *IEEE Roboti. Autom. Lett.* **7** 11 174–11 181
[23] Ng T J, Chen N and Zhang F 2023 Snapp: an agile robotic fish with 3-D maneuverability for open water swim *IEEE Robot. Autom. Lett.* **8** 6499–506
[24] Li Z, Ge L, Xu W and Du Y 2018 Turning characteristics of biomimetic robotic fish driven by two degrees of freedom of pectoral fins and flexible body/caudal fin *Int. J. Adv. Robot. Syst.* **15** 1729881417749950
[25] Tong R, Wu Z, Chen D, Wang J, Du S, Tan M and Yu J 2022 Design and optimization of an untethered high-performance robotic tuna *IEEE/ASME Trans. Mechatron.* **27** 4132–42
[26] Yu J, Liu L and Wang L 2006 Dynamics and control of turning maneuver for biomimetic robotic fish *2006 IEEE/RSJ Int. Conf. on Intelligent Robots and Systems* pp 5400–5
[27] Lauder G V and Drucker E G 2002 Forces, fishes and fluids: hydrodynamic mechanisms of aquatic locomotion *Physiology* **17** 235–40
[28] Domenici P and Blake R W 1997 The kinematics and performance of fish fast-start swimming *J. Exp. Biol.* **200** 1165–78
[29] Downs A M, Kolpas A, Block B A and Fish F E 2023 Multiple behaviors for turning performance of pacific bluefin tuna (Thunnus orientalis) *J. Exp. Biol.* **226** jeb244144
[30] Thandiackal R and Lauder G V 2020 How zebrafish turn: analysis of pressure force dynamics and mechanical work *J. Exp. Biol.* **223** jeb223230
[31] Mwaffo V, Zhang P, Cruz S R and Porfiri M 2017 Zebrafish swimming in the flow: a particle image velocimetry study *PeerJ* **5** e4041
[32] Zhong Q and Quinn D B 2021 Streamwise and lateral maneuvers of a fish-inspired hydrofoil *Bioinsp. Biomim.* **16** 056015
[33] Read D A, Hover F S and Triantafyllou M S 2003 Forces on oscillating foils for propulsion and maneuvering *J. Fluids Struct.* **17** 163–83
[34] Soltan K, O'Brien J, Dusek J, Berlinger F and Nagpal R 2018 Biomimetic actuation method for a miniature, low-cost multi-jointed robotic fish *OCEANS 2018 MTS/IEEE Charleston* pp 1–9
[35] Berlinger F, Saadat M, Haj-Hariri H, Lauder G V and Nagpal R 2021 Fish-like three-dimensional swimming with an autonomous, multi-fin and biomimetic robot *Bioinsp. Biomim.* **16** 026018
[36] Saro-Cortes V, Sedky G, Ko H, Flammang B and Wissa A 2023 Hydrodynamic evaluation of a flying fish robotic model organism: a study on the effects of the caudal fin shape *2023 IEEE Conf. on Control Technology and Applications (CCTA)* (IEEE) pp 670–4
[37] Di Santo V, Goerig E, Wainwright D K, Akanyeti O, Liao J C, Castro-Santos T and Lauder G V 2021 Convergence of undulatory swimming kinematics across a diversity of fishes *Proc. Natl Acad. Sci.* **118** e2113206118
[38] Gazzola M, Argentina M and Mahadevan L 2014 Scaling macroscopic aquatic locomotion *Nat. Phys.* **10** 758–61
[39] Zhang Y, Ko H, Calicchia M A, Ni R and Lauder G V 2024 Collective movement of schooling fish reduces the costs of locomotion in turbulent conditions *PLoS Biol.* **22** e3002501
[40] Anderson J M 2002 Maneuvering and stability performance of a robotic tuna *Integr. Comp. Biol.* **42** 118–26
[41] Chen X, Yu J, Wu Z, Meng Y and Kong S 2020 Toward a maneuverable miniature robotic fish equipped with a novel magnetic actuator system *IEEE Trans. Syst. Man Cybern.: Syst.* **50** 2327–37
[42] Katzschmann R K, DelPreto J, MacCurdy R and Rus D 2018 Exploration of underwater life with an acoustically controlled soft robotic fish *Sci. Robot.* **3** eaar3449
[43] Hu Y, Liang J and Wang T 2015 Mechatronic design and locomotion control of a robotic thunniform swimmer for fast cruising *Bioinsp. Biomim.* **10** 026006
[44] Ni D, Ko H and Nagpal R 2024 Leader-follower 3D formation for underwater robots (arXiv:2410.23128)